J. Fluid Mech. (1980), *vol.* 101, *part* 3, *pp.* 631–646
Printed in Great Britain

The numerical simulation of the steady movement of a fluid meniscus in a capillary tube

By JAMES LOWNDES†
Department of Mathematics, University of Manchester, Manchester M13 9PL

(Received 30 August 1979 and in revised form 4 June 1980)

The steady movement of a fluid meniscus in a circular capillary tube is analysed by means of finite-element numerical simulation for a range of values of contact angles and contact-line velocities with minute slippage of the fluid on the tube wall, thus relaxing the conventional no-slip boundary condition. The resulting flow field does not produce unbounded forces at contact line, contrary to that with the no-slip condition. The unknown meniscus shape is determined by an iterative scheme in which the imbalance in the normal-stress boundary condition is the basis for improving the shape. Comparison of the numerical results found here and the experimental results of a number of investigators suggests the possibility that the contact angle does not vary with contact-line velocity.

1. Introduction

Wetting and dewetting of solids by fluids involve the movement over solid surfaces of the solid/fluid/gas line of contact. A moving contact line can be found in many different situations; some cases in which it plays a central role are the spreading of adhesives, the flowing of lubricants into inaccessible locations, the coating of solid surfaces with a thin uniform layer of fluid and the displacement of oil by water through a porous medium.

To understand the dynamics of the contact-line movement we must solve the Navier–Stokes equation with applied boundary-conditions for the flow of fluid over the solid surface. However as shown by Moffatt (1964), Huh & Scriven (1971), and as discussed further by Dussan V. & Davis (1974), unbounded forces are then produced at the contact line. This singularity arises from the use of the conventional no-slip condition of fluid mechanics on the solid surface. Since, for the contact line to move, adjacent fluid elements must be brought to (or removed from) the solid surface. The adjacent elements then assume the velocity of the contact line, but at the same time they should not move on the solid surface, if we enforce the no-slip condition; doing this, however, creates a discontinuity in velocity at the contact line Dussan V. & Davis (1974).

This anomaly can be remedied in various ways (see Dussan V. 1976; Hocking 1976, 1977; Huh & Mason 1977). In this paper we consider the most widely used remedy and permit the fluid to slip along the solid surface. The theoretical justification for the replacement of the no-slip condition by a slip condition, in problems involving a

† Present address: Ferranti Computer Systems Ltd., Bird Hall Lane, Cheadle Heath, Stockport SK3 0XQ.

0022-1120/80/4647-2690 $02.00

moving contact line, was discussed by Hocking (1976). Note however, that no relevant experiments have been performed to document slip for flow near a moving contact line. Of course the slip condition must become the conventional, and proved experimentally, no-slip condition away from the moving contact line.

To study the possibility of slippage near to the moving contact line, Huh & Mason (1977) considered the steady movement of a fluid meniscus displacing air or its own vapour in a circular capillary. However, they restricted their study to the systems for which the meniscus shape is approximately flat everywhere. In § 2 we consider the problem with a more general meniscus shape. The solutions are generated by the finite-element method, which has advantages over other available methods, as discussed in § 3. The iterative scheme used to determine the meniscus shape is described in § 4. The results are discussed in § 5. We shall be concerned primarily with the shape of the meniscus since the velocity and pressure fields exhibit similar features to those obtained by Huh & Mason (1977) for the flat meniscus. In particular, the present work is based on the assumption that the contact angle θ_c (defined as the angle formed by the meniscus and the solid surface at the moving contact line) does not vary with contact-line velocity, and this assumption is supported by the comparison between calculated and experimentally observed meniscus shapes.

2. Capillary flow

Consider the steady movement of a fluid meniscus displacing air or its own vapour in a circular capillary. The tube radius a is sufficiently small that the effect of gravity is negligible i.e. $\rho g a^2/\gamma \ll 1$, where ρ is the fluid density, g is the acceleration due to gravity and γ is the fluid/gas interfacial tension. To express the hydrodynamic problem of the meniscus movement in a convenient mathematical form, we assume that all dependent and independent variables have been non-dimensionalized with respect to the tube radius a, the contact-line velocity U and a characteristic pressure $\mu U/a$, where μ is the fluid viscosity. By virtue of the axial symmetry of the meniscus, it can be described by $x_2 = h(x_1)$ in cylindrical co-ordinates x_i moving with the meniscus (see figure 1), where $h(0) = 0$. If the Reynolds number $\rho a U/\mu$ is small (in this paper it is always less than 10^{-2}), the flow field behind the meniscus formed by an incompressible Newtonian fluid can be determined by solving the creeping-flow approximation to the Navier–Stokes equation

$$\sigma_{ik,k} = 0, \tag{2.1}$$

where $(\,)_{,i}$ denotes covariant differentiation with respect to x_i, the usual summation convention is employed for repeated indices, σ_{ij} is the stress tensor with components

$$\sigma_{ij} = -p\delta_{ij} + (u_{i,j} + u_{j,i}), \tag{2.2}$$

p is the fluid pressure, δ_{ij} are the components of the unit tensor and u_i are the velocity components in the x_i co-ordinates. In this notation the continuity equation can be written as

$$u_{k,k} = 0. \tag{2.3}$$

The boundary conditions to be applied to the coupled system (2.1) to (2.3) are as follows (see figure 2):

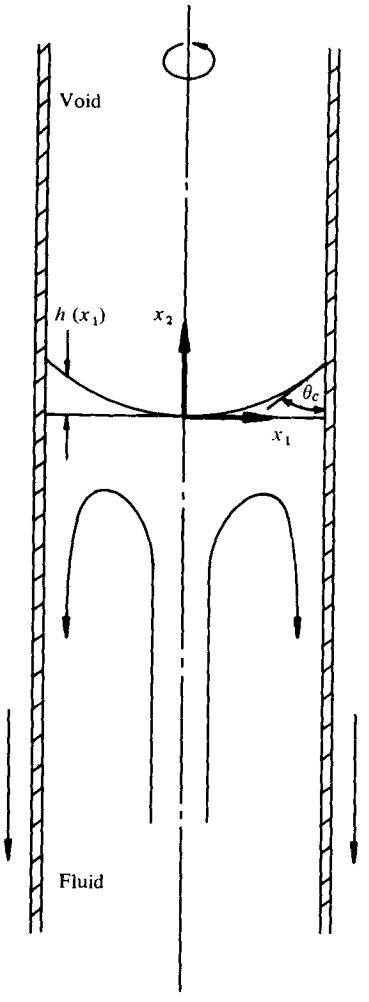

FIGURE 1. Schematic diagram of a fluid meniscus moving steadily in a circular capillary tube.

(i) Vanishing normal component of fluid velocity on the tube wall:

$$u_1 = 0 \quad \text{on} \quad x_1 = 1. \tag{2.4}$$

(ii) The slip condition to be applied on the tube wall is the classical slippage boundary condition that the slip velocity is proportional to the shear stress exerted on the tube wall:

$$\sigma_{12} = -\frac{2}{\epsilon}(1+u_2) \quad \text{on} \quad x_1 = 1, \tag{2.5}$$

where $\epsilon = l/a$ and l is the characteristic length which provides an indication of the size of the region near to the contact line where slip is important. Different slip conditions have been used by Dussan V. (1976) and Huh & Mason (1977), however, they showed that, while many differences exist on the slip length scale for the different conditions, few, if any, are perceptible on the meniscus length scale, provided $\epsilon \ll 1$.

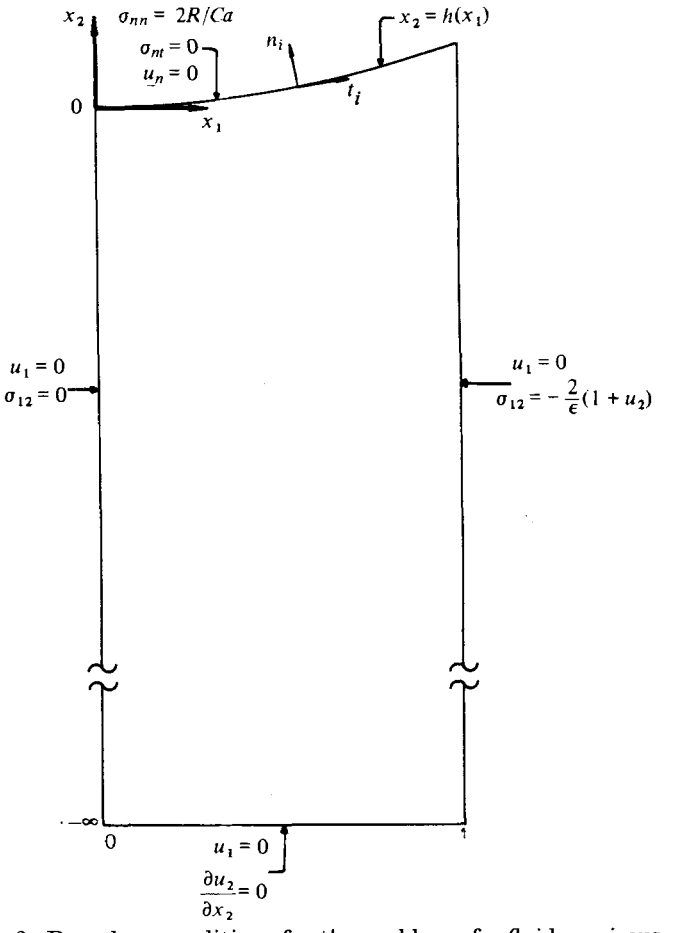

FIGURE 2. Boundary conditions for the problem of a fluid meniscus moving steadily in a circular capillary tube.

(iii) Vanishing normal component of fluid velocity on the meniscus:

$$u_n (\equiv u_k n_k) = 0 \quad \text{on} \quad x_2 = h, \tag{2.6}$$

where n_i is the normal to the meniscus.

(iv) Vanishing tangential stress on the meniscus:

$$\sigma_{nt} (\equiv n_j \sigma_{jk} t_k) = 0 \quad \text{on} \quad x_2 = h, \tag{2.7}$$

where t_i is the tangent to the meniscus.

(v) Balancing of the normal stress and the capillary pressure on the meniscus:

$$\sigma_{nn} (\equiv n_j \sigma_{jk} n_k) = \frac{2R}{Ca} \quad \text{on} \quad x_2 = h, \tag{2.8}$$

where Ca is the capillary number $\mu U/\gamma$ (a ratio of viscous to surface forces) and R is the mean curvature of the meniscus.

(vi) Vanishing normal component of fluid velocity on the tube centre-line:

$$u_1 = 0 \quad \text{on} \quad x_1 = 0. \tag{2.9}$$

(vii) Vanishing tangential stress on the tube centre-line:

$$\sigma_{12} = 0 \quad \text{on} \quad x_1 = 0. \tag{2.10}$$

(viii) Vanishing radial component of fluid velocity at a large distance upstream:

$$u_1 = 0 \quad \text{as} \quad x_2 \to -\infty. \tag{2.11}$$

(ix) Vanishing axial component of axial fluid velocity gradient at a large distance upstream:

$$\frac{\partial u_2}{\partial x_2} = 0 \quad \text{as} \quad x_2 \to -\infty. \tag{2.12}$$

The numerical solution procedure used to solve the coupled system (2.1) to (2.3) with applied boundary conditions (2.4) to (2.12), is described in the following section and is a particular formulation of the general method known as the finite-element method.

3. Finite-element formulation

In the finite-element method, the flow domain is divided into geometrically simple subdomains (elements), usually triangles or quadrilaterals. Within each element a number of points, called nodes, are identified. The dependent variables are approximated locally over the element by continuous functions, usually low-order polynomials, defined in terms of the values of the dependent variables at the nodes. A set of equations for the nodal point unknowns of each element are found by using a Galerkin weighted residual method in which the error resulting from the substitution of the approximate functions into the governing differential equations, is distributed over the whole flow domain. This distribution is such that, on average, the partial differential equations are obeyed. Finally, an assembly of the elements and their corresponding equations through the connexion of appropriate nodes yields a discrete analogue to the original continuous problem.

For a general discussion of the finite-element method, with applications to continuum mechanics, see for example Zienkiewicz (1977) and Desai & Abel (1972); and more specifically for fluid mechanical applications, see for example Chung (1978), Oden *et al.* (1974) and Taylor, Morgan & Brebbia (1978).

The finite-element method has aspects which suit it well to the problem considered here. First, the elements need not have uniform size and shape, so that irregular domains, those bounded by other than co-ordinate surfaces, require no special handling, a significant advantage for free-surface flow problems, which by their nature occur on irregular domains. In addition, the fact that element sizes need not be uniform means that computational power can be deployed efficiently by using small elements in regions of rapid variations of the dependent variables, near to the contact line for instance, and large ones elsewhere. Second, the slippage boundary condition on the tube wall (2.5) and the vanishing tangential stress on the meniscus (2.7) and on the tube centre-line (2.10) enter into the finite-element method in a particularly simple way. Separately constructed approximations to such boundary conditions are not required as they are in finite-difference methods. The price to be paid for these advantages is the complexity of the resulting computer programs, which are substantially more difficult to develop than corresponding finite-difference programs.

Due to the local nature of the approximation of the dependent variables, each element may be considered individually for purposes of equation formulation. For the present problem let the velocity and pressure be represented within an element by

$$u_i = \phi_\alpha u_{\alpha i}, \quad p = \psi_\alpha p_\alpha, \tag{3.1), (3.2}$$

where $u_{\alpha i}$ and p_α are the values of u_i and p respectively at node α, ϕ_α and ψ_α are the corresponding interpolation functions and for each element the Greek indices take values up to a maximum of the number of local nodes associated with a particular quantity (for the element we shall use these maxima are 6 for the velocity components and 3 for the pressure). The only conditions imposed on the interpolating functions are to ensure that the dependent variables are compatible at the interface between two elements (see for example Desai & Abel 1972, p. 178). These conditions are automatically satisfied for the polynomials used in the ensuing analysis.

Introducing relations (3.1) and (3.2) into equations (2.1) and (2.3) yields residuals, corresponding to each equation, since in general the equations will not be satisfied identically. We can guarantee that the residual of each equation vanishes in an average sense over the element by requiring that it is orthogonal to the sub-space spanned by the interpolation function of the dependent variable associated with that equation, a Galerkin weighted residual method. The Galerkin weighted residual equations corresponding to equations (2.1) and (2.3) are

$$\int_V \phi_\alpha \sigma_{ik,k} dV = 0, \tag{3.3}$$

$$\int_V \psi_\alpha u_{k,k} dV = 0, \tag{3.4}$$

where V is the volume of the element. Use of the divergence theorem on equation (3.3) yields

$$\int_V \phi_{\alpha,k} \sigma_{ik} dV - \int_{\partial V} \phi_\alpha \sigma_{ik} n_k dS = 0, \tag{3.5}$$

where ∂V is the boundary of the element and n_i is the outward-pointing normal unit vector on ∂V. The primary reason for applying the divergence theorem is to enable us to apply the boundary conditions (2.5), (2.7) and (2.10) in a particularly simple way. It also lowers the order of the highest derivative and so requires a degree less of continuity in the interpolation functions, and is numerically more sound.

If we now introduce equations (2.2), (3.1) and (3.2) into equations (3.4) and (3.5), we obtain the following linear algebraic equations associated with each element in the flow field

$$\int_V (\phi_{\alpha,k}\phi_{\beta,k} u_{\beta i} + \phi_{\alpha,k}\phi_{\beta,i} u_{\beta k} - \phi_{\alpha,i}\psi_\beta p_\beta) dV = \int_{\partial V} \phi_\alpha \sigma_{ik} n_k dS, \tag{3.6}$$

$$\int_V \psi_\alpha \phi_{\beta,k} u_{\beta k} dV = 0. \tag{3.7}$$

We can rewrite the equations (3.6) and (3.7) in the following form

$$M_{\alpha i \beta k} u_{\beta k} - H_{\alpha i \beta} p_\beta = I_{\alpha i}, \tag{3.8}$$

$$H_{\beta k \alpha} u_{\beta k} = 0, \tag{3.9}$$

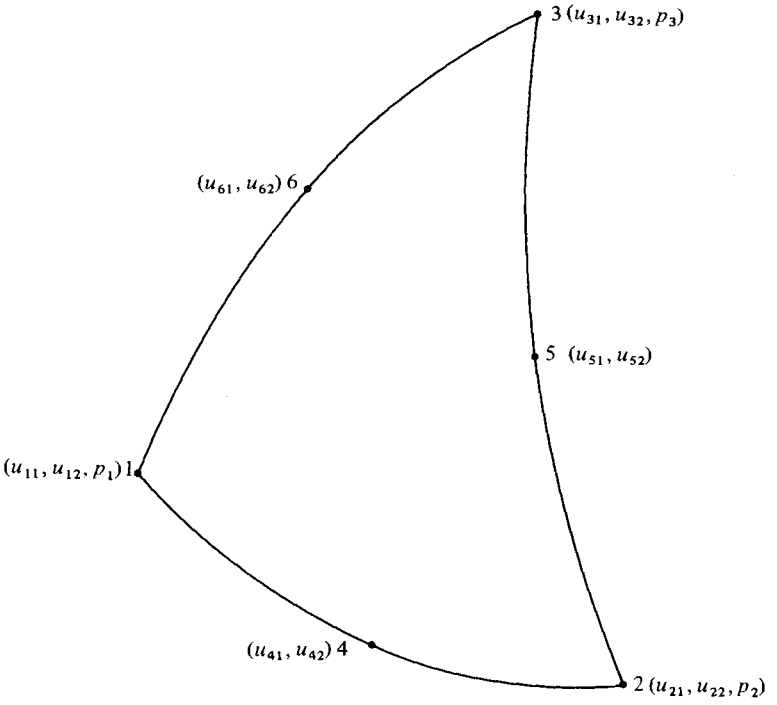

FIGURE 3. Basic triangular subelement nodal variables.

where

$$M_{\alpha i\beta j} = \int_V \phi_{\alpha,k}\phi_{\beta,k}\delta_{ij}\,dV + \int_V \phi_{\alpha,j}\phi_{\beta,i}\,dV, \tag{3.10}$$

$$H_{\alpha i\beta} = \int_V \phi_{\alpha,i}\psi_\beta\,dV, \tag{3.11}$$

$$I_{\alpha i} = \int_{\partial V} \phi_\alpha \sigma_{ik} n_k\,dS. \tag{3.12}$$

The above derivation has been concerned with a single finite-element and the limited portion of the flow domain it represents. The discrete representation of the entire flow domain is obtained through an assemblage of elements such that inter-element continuity of the approximate velocity components and pressure is enforced. This continuity requirement is met through the appropriate summation of equations for nodes common to adjacent elements (the so-called 'direct stiffness' approach Zienkiewicz 1977). The result of such an assembly process is a system of matrix equations of the form given by equations (3.8) and (3.9). Note that the assembled form of the surface integral on the element boundary on the right-hand side of equation (3.8) is a surface integral on the boundary of the entire flow domain.

The various boundary conditions for the present problem (2.4) to (2.12), are applied to the assembled equations in two distinct ways. The boundary conditions (2.4), (2.6), (2.9) and (2.11) are applied by replacing the equations for the particular degrees of freedom by equations enforcing the boundary conditions. In contrast, the boundary conditions (2.5), (2.7), (2.8), (2.10) and (2.12) are applied by substituting them in the

surface integral on those element boundaries making up the part of the boundary of the flow domain where the boundary conditions are specified. Hence, the boundary conditions (2.4) to (2.12) enter into the finite-element formulation in a particularly simple way.

The solution of the assembled unsymmetric banded linear algebraic equations for all nodal values of the velocity components and pressure is undertaken, using the variable-bandwidth band solution form of the Gaussian elimination method (see for example Zienkiewicz 1977, p. 718). For efficiency the assemblage and elimination processes are performed simultaneously. This is done by processing the nodes in a prescribed order so that the equations are eliminated as soon as they are completely formed.

The basic finite-element used for the present problem is a 13 node, 31-degrees of-freedom quadrilateral (the elements are actually axisymmetric rings with quadrilateral cross-section) composed of four six-node, 15-degrees-of-freedom triangles. Within each triangular subelement, the velocity components u_i are approximated using a quadratic interpolation function and the pressure p is approximated by a linear interpolation function. The arrangement of the nodal point variables is shown in figure 3. The interpolation functions for each triangular subelement are given by

$$\phi_\alpha = \begin{Bmatrix} L_1(2L_1-1) \\ L_2(2L_2-1) \\ L_3(2L_3-1) \\ 4L_1L_2 \\ 4L_2L_3 \\ 4L_3L_1 \end{Bmatrix}, \tag{3.13}$$

$$\psi_\alpha = \begin{Bmatrix} L_1 \\ L_2 \\ L_3 \end{Bmatrix}, \tag{3.14}$$

where the ordering of the functions corresponds to the ordering of the unknowns shown in figure 3. The interpolation functions in equations (3.13) and (3.14) are expressed in terms of the natural or area co-ordinates for a triangle, L_i (see for example Zienkiewicz 1977, p. 165). Note that the natural co-ordinates L_i are not independent but are related by

$$L_1 + L_2 + L_3 = 1. \tag{3.15}$$

The co-ordinate transformation between the physical co-ordinates x_i and the natural co-ordinates L_i is obtained from the parametric concept discussed by Ergatoudis, Irons and Zienkiewicz (1968). Although this transformation can be quite general we shall restrict ourselves to the particular case of an isoparametric element where the interpolation functions defining the dependent variables are of the same order as the interpolation functions defining the element geometry. That is, the co-ordinate transformation is given by

$$x_i = \phi_\alpha x_{\alpha i}, \tag{3.16}$$

where $x_{\alpha i}$ are the values of x_i at node α. In particular, a quadratic interpolation of the element boundary is possible and hence, the element boundaries can closely follow

those meniscus profiles found in the present problem. The construction of the element matrices defined by equations (3.10) and (3.11) requires the computation of various derivatives and integrals of the interpolation functions given in equations (3.13) and (3.14). Since the interpolation functions are given in terms of the natural co-ordinates L_i and the derivatives and integrals are in terms of the physical co-ordinates x_i the following relations need to be defined

$$\begin{aligned}\frac{\partial \phi_\alpha}{\partial L_i} &= \frac{\partial x_k}{\partial L_i}\phi_{\alpha,k} \quad (i = 1, 2)\\ &= \frac{\partial}{\partial L_i}(\phi_\beta x_{\beta k})\,\phi_{\alpha,k}\\ &= J_{ik}\phi_{\alpha,k},\end{aligned} \tag{3.17}$$

where L_3 has been expressed in terms of L_1 and L_2 using equation (3.15) and

$$J_{ij} = x_{\beta j}\frac{\partial \phi_\beta}{\partial L_i} \tag{3.18}$$

is the Jacobian matrix of the transformation. Inverting the Jacobian matrix provides the needed relation for the derivatives of the interpolation functions

$$\phi_{\alpha,i} = J^{-1}_{ik}\frac{\partial \phi_\alpha}{\partial L_k}. \tag{3.19}$$

To complete the transformation from physical co-ordinates x_i to natural co-ordinates L_i, the expression for an elemental volume is required. This is given by

$$\begin{aligned}dV &= x_1\,dx_1\,dx_2\,dx_3\\ &= \phi_\beta x_{\beta 1}\det J_{ij}\,dL_1\,dL_2\,dx_3,\end{aligned} \tag{3.20}$$

where x_3 is the circumferential co-ordinate of the cylindrical co-ordinates x_i and det indicates the determinant of a matrix. Use of the relations given in equations (3.19) and (3.20) allows the element matrices defined by equations (3.10) and (3.11) to be expressed as integrals of rational functions in the L_i co-ordinate system. The evaluation of such integrals requires a numerical quadrature procedure and the Gauss–Radau formula is used (see for example Zienkiewicz 1977, p. 200). After assembling the equations from the four triangles, using the 'direct stiffness' approach described previously, the eleven interior degrees of freedom associated with the common side nodes and the quadrilateral centroid are condensed numerically from the system, resulting in substantial computational savings, and are then found after the solution has been obtained for the retained degrees of freedom.

If one attempts to use equal order interpolation for the velocity components and pressure, then a singular system of equations arises Schneider, Raithby & Yovanovich (1978). It was demonstrated in Schneider *et al.* (1978) that the emergence of the singular system of equations results from the application of boundary conditions to the finite-element equations. The flexibility to interpolate pressure to an equal or perhaps higher order than the velocity components can be gained by replacing the continuity equation (2.3) by a Poisson equation, obtained by taking the curl of the vector equation (2.1) and using the continuity equation (2.3), for pressure Schneider *et al.* (1978).

4. Meniscus profile scheme

Since the meniscus profile is not known *a priori*, some sort of iterative scheme is needed to determine it. When motion is steady the three boundary conditions on the meniscus are given by equations (2.6) to (2.8), that is, (i) no normal component of fluid velocity on the meniscus, (ii) no tangential stress on the meniscus and (iii) balancing of normal stress and capillary pressure on the meniscus. All iterative schemes employ a similar strategy. First a profile of the meniscus is chosen, either by an informed guess or on the basis of the previous iterations. The Navier–Stokes and continuity equations are solved for the velocity and pressure fields in the fluid, but only two of the three boundary conditions on the meniscus are satisfied. The third boundary condition is then used to decide how to alter the meniscus profile, and the process is repeated to convergence. A fuller discussion of the various schemes, with references, can be found in Orr & Scriven (1978).

The iterative scheme employed in the present work is a normal-stress scheme in which the imbalance in the normal-stress boundary condition is the basis for improving the meniscus profile. Before describing the iterative scheme in detail we derive a form of the normal-stress boundary condition (2.8) which is particularly well suited for the present problem.

Substituting an expression for the mean curvature of the meniscus (see Huh & Mason 1977) in the normal-stress boundary condition (2.8) gives

$$\sigma_{nn} = \frac{1}{Ca}\left\{\frac{d^2h/dx_1^2}{[1+(dh/dx_1)^2]^{\frac{3}{2}}} + \frac{(1/x_1)(dh/dx_1)}{[1+(dh/dx_1)^2]^{\frac{1}{2}}}\right\} \quad \text{on} \quad x_2 = h. \tag{4.1}$$

If θ denotes the angle at a given value of x_1 between a tangent line to the meniscus profile and a line parallel to the tube wall, then

$$\frac{dh}{dx_1} = \cot\theta \tag{4.2}$$

and equation (4.1) can be written as

$$\sigma_{nn} = \frac{1}{Ca}\frac{1}{x_1}\frac{d}{dx_1}(x_1\cos\theta) \quad \text{on} \quad x_2 = h. \tag{4.3}$$

Integrating equation (4.2) with respect to x_1 and using the boundary conditions $\cos\theta = 0$ and $h = 0$ on $x_1 = 0$, and multiplying equation (4.3) by x_1 and integrating with respect to x_1, we obtain for the equation for the meniscus profile

$$h(x_1) = \int_0^{x_1} \cot\theta\, dx_1', \tag{4.4}$$

where

$$\cos\theta = \frac{Ca}{x_1}\int_0^{x_1} x_1'\sigma_{nn}\, dx_1'. \tag{4.5}$$

The normal-stress iterative scheme used to determine the meniscus profile is as follows.

(1) Guess a meniscus profile. In the present work this was a flat meniscus profile.

(2) Solve the Navier–Stokes and continuity equations for the velocity and pressure in the fluid, imposing only the boundary conditions (2.4) to (2.7) and (2.9) to (2.12).

(3) Calculate the values of the normal stress of the fluid on the meniscus σ_{nn} at discrete values of x_1. Note that the pressure, and as a consequence σ_{nn}, is determined only up to a constant since it does not appear in any of the applied boundary conditions. However, using the boundary condition $\theta = \theta_c$ on $x_1 = 1$, equation (4.5) gives

$$\cos\theta_c = Ca\int_0^1 x_1'\sigma_{nn}\,dx_1' \tag{4.6}$$

and this integral constraint sets the level of σ_{nn}, and hence the pressure, in the flow field.

(4) Use the values of σ_{nn} to integrate (4.4) and (4.5) numerically, and thereby obtain a new meniscus profile.

(5) Repeat steps (2) to (4) until the change in meniscus profile is below a specified tolerance.

The above iterative scheme generated convergent solutions for all cases attempted (see § 5). Usually three to five iterations were sufficient to reduce the maximum change in any of the meniscus nodes to less than 10^{-4}.

5. Results and discussion

To calculate the flow field and the meniscus profile for the fluid/solid systems which have been employed in the literature, using the numerical techniques described in §§ 3 and 4, we must know the slip length l (see equation (2.5)) for the systems. It should be possible to determine the appropriate value of l for a given system by using the theoretical analysis to predict some measurable physical quantities, for example the force on a length of tube in contact with the fluid. Because this value is not available, we shall be consistent with the work of Huh & Mason (1977) and set l equal to a lower bound of 10^{-7} cm (that is, the average diameter of a fluid molecule). This choice of l gives the largest possible deformation due to viscous forces. For completeness, we also consider the effect, on the meniscus profile for a particular system, of varying l.

It should be noted that a semi-infinite flow domain must be dealt with in the present problem. In order to economize on the size of the flow domain to be computed, we have used knowledge of the analytical solutions obtained for a flat meniscus profile (Huh & Mason 1977). These analytical solutions suggest that the computational flow domain need only extend to a distance of one tube diameter upstream of the part of the meniscus with the minimum value of h. Note that the boundary conditions (2.11) and (2.12) are then applied to this computational flow domain. This distance of one diameter tube has also been verified for flat and also more general meniscus profiles by numerical experimentation.

A typical finite-element mesh used in the numerical computations is illustrated in figure 4. This mesh was established based on the expected behaviour of the solution. From the work of Huh & Mason (1977) it is known for a flat meniscus profile that at the contact line the pressure and velocity gradients have a weak singularity varying as the logarithm of the distance from the contact line. For the triangular subelements, which interpolate both the pressure and velocity gradients linearly over each element, to represent the solution adequately it is clear that the elements must become

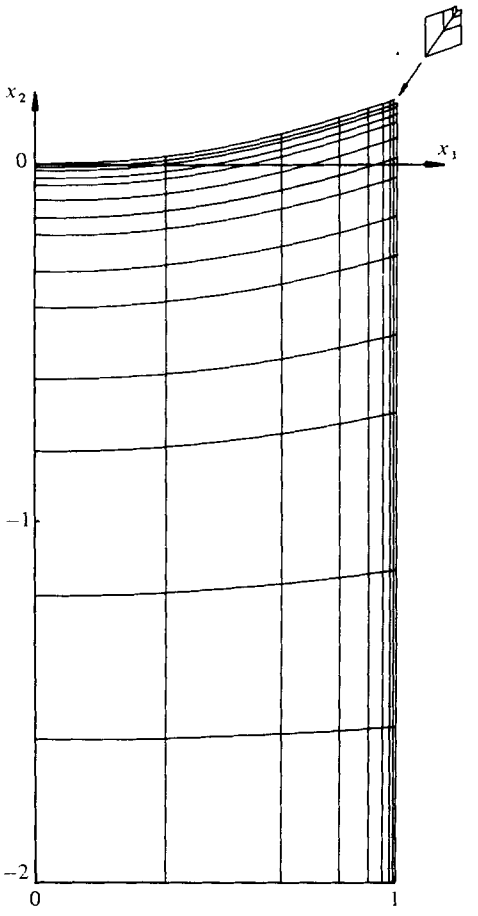

FIGURE 4. Finite-element mesh pattern for $\theta_e = 69°$, $a = 0{\cdot}978$ mm, $l = 10^{-7}$ cm, $Ca = 0$. The first three levels of local mesh refinement near to the contact line are shown to 10 times the scale of the remainder of the mesh.

progressively smaller the nearer they are to the contact line. This was accomplished using a systematic local mesh refinement scheme. The number of levels of local refinement (only the first three levels are shown in figure 4) is dependent on the value of ϵ, and should be such that the meniscus profile is unchanged for further levels of refinement. In general it was found that the smallest element should have a size at least four orders of magnitude less than ϵ.

In the numerical computations we assume, for reasons that will be apparent later, that the contact angle θ_c for a particular system does not vary with contact-line velocity. The values of the relevant physical quantities θ_c, a and Ca, are those from experiments conducted by Rose & Heins (1962), Hansen & Toong (1971*a*) and Hoffman (1975). Figure 5 shows the meniscus profiles for various values of θ_c, a and Ca. The profiles are good approximations to those found in the experiments. Figure 6 shows the corresponding values of the meniscus slope. Clearly the slope is a strong function of x_1 near to the contact line in the dynamic cases. Figure 7 shows the meniscus profile

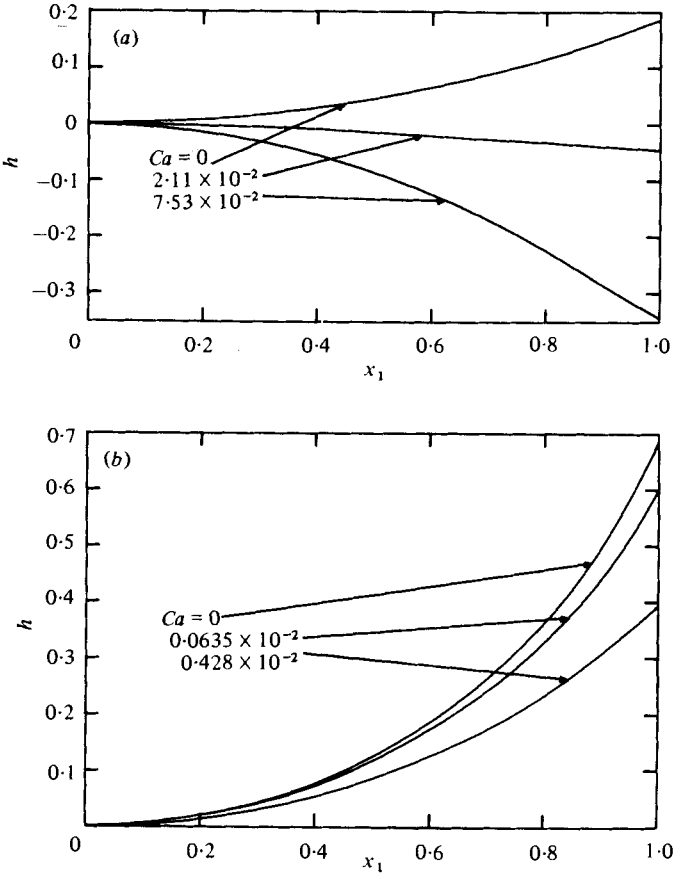

FIGURE 5. Meniscus profiles for (*a*) $\theta_c = 69°$, $a = 0{\cdot}978$ mm, $l = 10^{-7}$ cm and (*b*) $\theta_c = 21°$, $a = 1{\cdot}19$ mm, $l = 10^{-7}$ cm.

and meniscus slope for a range of values of l, for a particular set of values of θ_c, a and Ca. It is clear that the profile is sensitive to the magnitude of l.

In many experimental studies the contact angle was measured as a function of contact-line velocity. The commonest method of contact-angle measurement has been used, for instance, by Rose & Heins (1962), Hansen & Toong (1971*a*) and Hoffman (1975). The axial distance $h(1)$ between the centre-line position of the meniscus and the contact line is first measured on photographs of the meniscus. The meniscus is then assumed to be approximated by a spherical sector which has the same axial position as the meniscus at the tube centre-line and wall. Therefore, the 'measured contact angle', $\theta_M^{\exp}$, is defined to be the angle formed by this spherical sector and the tube wall at the tube wall and is given by the equation

$$\theta_M^{\exp} = \cos^{-1}\left\{\frac{2h(1)}{1+[h(1)]^2}\right\}. \tag{5.1}$$

One unsettling question is whether or not the measured $\theta_M^{\exp}$ was indeed the real contact angle θ_c. If severe deformation of the meniscus occurs near to the contact line

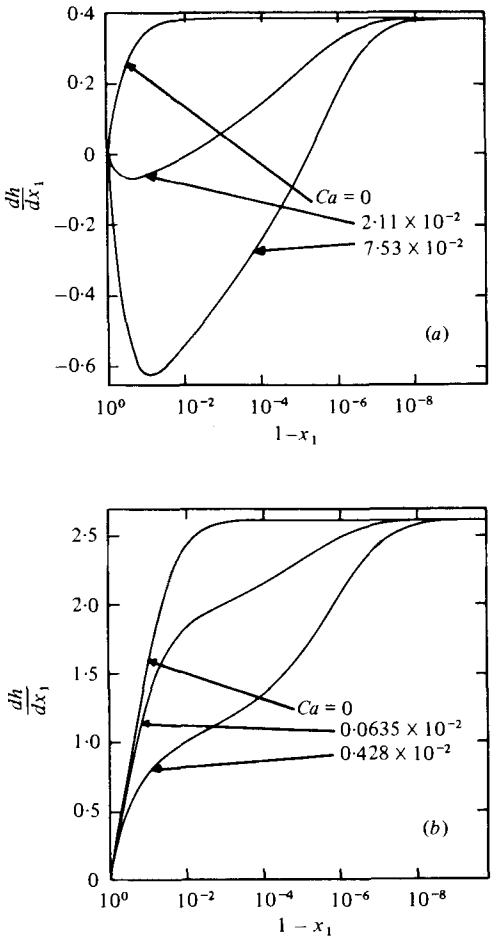

FIGURE 6. Meniscus slope for (*a*) $\theta_c = 69°$, $a = 0{\cdot}978$ mm, $l = 10^{-7}$ cm and (*b*) $\theta_c = 21°$, $a = 1{\cdot}19$ mm, $l = 10^{-7}$ cm.

(at a distance from the line at which it is impossible to detect experimentally, that is, less than 10^{-4} cm) owing to viscous forces, as Hansen & Toong (1971*b*) pointed out, the meniscus will no longer be approximated by a spherical sector there and the significance of the contact-angle measurements will therefore be in doubt.

A comparison of the values found in the numerical calculations $\theta_M^{\text{cal}} - \theta_c$ (where we have assumed that the real contact angle θ_c does not vary with contact-line velocity and also that $l = 10^{-7}$ cm, and we have used equation (5.1) to define θ_M^{cal}) and observed in experiments $\theta_M^{\text{exp}} - \theta_c$ are shown in table 1 for the experimental data of Rose & Heins (1962), Hansen & Toong (1971*a*) and Hoffman (1975). The values $\theta_M^{\text{cal}} - \theta_c$ are good approximations to $\theta_M^{\text{exp}} - \theta_c$, which supports the assumption that the real contact angle does not vary with contact-line velocity and also suggests that θ_M^{exp}, which was measured as the real contact angle, was in fact an apparent contact angle. Of course, this may not be the case for all fluid/solid systems.

The possibility that θ_M^{exp} is only an apparent contact angle and that the real contact angle does not vary with contact-line velocity, has already been discussed by Huh & Mason (1977). In table 1, we also list the values $\theta_M^{\text{cal}} - \theta_c$ calculated by Huh & Mason.

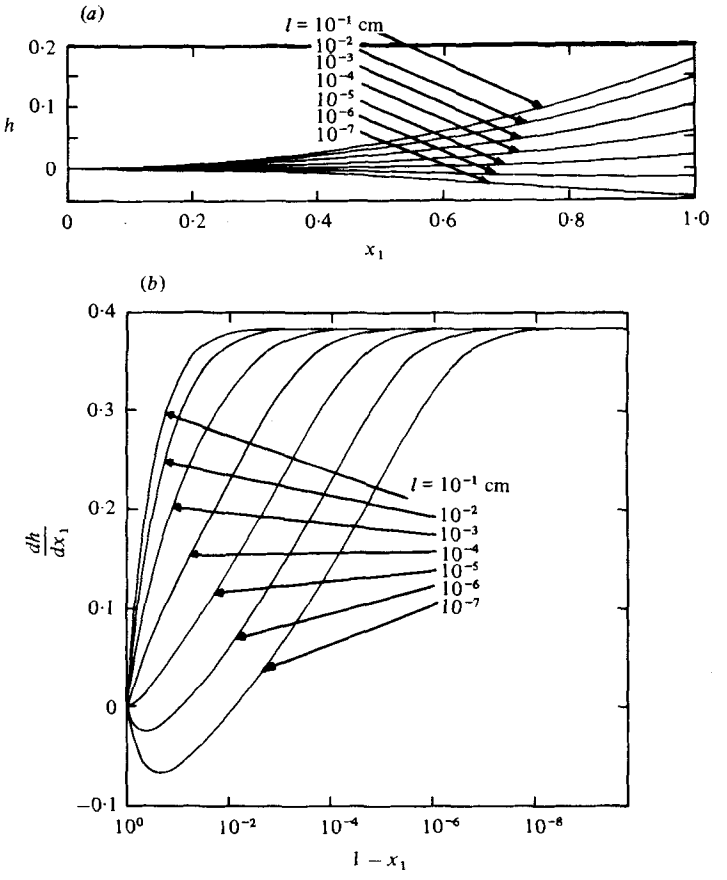

FIGURE 7. (*a*) Meniscus profiles and (*b*) meniscus slope for $\theta_c = 69°$, $a = 0{\cdot}978$ mm, $Ca = 0{\cdot}0211$.

For the first two systems in table 1, Huh & Mason agree with the conclusions reached in the present work. However, they wrongly conclude for the last two systems in table 1, using an expression that they admit is strictly inappropriate for such systems with low values of $\theta_M^{\exp}$ (because it was derived from expressions for the velocity and pressure fields obtained for a flat meniscus profile), that the real contact angle varies with contact-line velocity. Note that, the Huh & Mason definition of θ_M^{cal} differs slightly from that of equation (5.1). They effectively assume that the meniscus can be approximated by a spherical sector which has the same radius and axial position as the meniscus at the tube centre-line. Therefore, Huh & Mason effectively define θ_M^{cal} to be the angle formed by this spherical sector and the tube wall at the tube wall. Since the meniscus is an exact spherical sector only in the static case, it is inevitable that the two definitions are not equivalent. However, it can be shown, for the systems and values of Ca used in table 1, that the difference between the values of θ_M^{cal} for the two definitions is small. In fact, in the numerical calculations for table 1 the percentage difference between the values of θ_M^{cal} for the two definitions increased with Ca for a particular system and ranged from 0·9 % to 3·6 %.

I should like to thank the Science Research Council for financial support.

System	$Ca \times 10^3$	Calculated $\theta_M^{cal} - \theta_c$ (Present work) (°)	Experimental $\theta_M^{exp} - \theta_c$ (°)	Calculated $\theta_M^{cal} - \theta_c$ (Huh & Mason 1977) (°)
Admex 760/air/glass	2·11	26	21	23
$\theta_c = 69°$, $a = 0{\cdot}978$ mm	4·94	45	45	54
(Hoffman 1975)	5·16	46	42	56
	7·38	58	45	81
	7·53	59	47	82
Santicizer 405/air/glass	0·48	8·2	1·7	5·2
$\theta_c = 67°$, $a = 0{\cdot}978$ mm	0·89	14	8·2	9·7
(Hoffman 1975)	1·36	20	18	15
	4·36	43	48	48
	6·79	56	54	74
Nujol/air/glass	0·0635	7·3	4·8	0·7
$\theta_c = 21°$, $a = 1{\cdot}19$ mm	0·132	13	10	1·5
(Hansen & Toong 1971*a*)	0·196	16	13	2·2
	0·330	22	18	3·7
	0·428	26	20	4·7
Nujol/air/glass	0·140	11	11	1·4
$\theta_c = 23°$, $a = 0{\cdot}33$ mm	0·279	17	20	2·8
(Rose & Heins 1962)	0·419	23	27	4·2
	0·558	27	34	5·7
	0·698	31	42	7·1

TABLE 1. Comparison of the values of the measured contact angle calculated in the theoretical analyses of the present work and Huh & Mason (1977) ($l = 10^{-7}$ cm) and those observed in experiments.

REFERENCES

CHUNG, T. J. 1978 *Finite Element Analysis in Fluid Mechanics*. McGraw-Hill.

DESAI, C. S. & ABEL, J. F. 1972 *Introduction to the Finite Element Method*. Reinhold: Van Nostrand.

DUSSAN V., E. B. 1976 *J. Fluid Mech.* **77**, 665.

DUSSAN V., E. B. & DAVIS, S. H. 1974 *J. Fluid Mech.* **65**, 71.

ERGATOUDIS, I., IRONS, B. M. & ZIENKIEWICZ, O. C. 1968 *Int. J. Solids Structures* **4**, 31.

HANSEN, R. J. & TOONG, T. Y. 1971*a* *J. Colloid Interface Sci.* **36**, 410.

HANSEN, R. J. & TOONG, T. Y. 1971*b* *J. Colloid Interface Sci.* **37**, 196.

HOCKING, L. M. 1976 *J. Fluid Mech.* **76**, 801.

HOCKING, L. M. 1977 *J. Fluid Mech.* **79**, 209.

HOFFMAN, R. L. 1975 *J. Colloid Interface Sci.* **50**, 228.

HUH, C. & MASON, S. G. 1977 *J. Fluid Mech.* **81**, 401.

HUH, C. & SCRIVEN, L. E. 1971 *J. Colloid Interface Sci.* **35**, 85.

MOFFATT, H. K. 1964 *J. Fluid Mech.* **18**, 1.

ODEN, J. T., ZIENKIEWICZ, O. C., GALLAGHER, R. H. & TAYLOR, C. 1974 *Finite Element Methods in Flow Problems*. University of Alabama Press, Huntsville.

ORR, F. M. & SCRIVEN, L. E. 1978 *J. Fluid Mech.* **84**, 145.

ROSE, W. & HEINS, R. W. 1962 *J. Colloid Sci.* **17**, 39.

SCHNEIDER, G. E., RAITHBY, G. D. & YOVANOVICH, M. M. 1978 In *Numerical Methods in Laminar and Turbulent Flow* (ed. C. Taylor, K. Morgan & C. A. Brebbia), p. 89. Plymouth: Pentech.

TAYLOR, C., MORGAN, K. & BREBBIA, C. A. 1978 *Numerical Methods in Laminar and Turbulent Flow*. Plymouth: Pentech.

ZIENKIEWICZ, O. C. 1977 *The Finite Element Method*. McGraw-Hill.